Surface & Coatings Technology 374 (2019) 845–851

Contents lists available at ScienceDirect

Surface & Coatings Technology

journal homepage: www.elsevier.com/locate/surfcoat

On the possibility of synthesizing multilayered coatings in the (Ti,Al)N system by RGPP: A microstructural study

A. El Mouatassim[a,b], M.-J. Pac[a,*], F. Pailloux[b], G. Amiard[b], P. Henry[a], C. Rousselot[c], D. Eyidi[b], M.-H. Tuilier[a,1], T. Cabioc'h[b]

[a] Université de Haute Alsace, Laboratoire de Physique et Mécanique Textiles (EA 4365), F-68093 Mulhouse, France
[b] Institut Pprime, UPR 3346, Université de Poitiers-ENSMA, SP2MI, Téléport 2-BP 30179, 86962 Futuroscope Chasseneuil Cedex, France
[c] Université de Bourgogne Franche-Comté, Institut FEMTO ST, CNRS, UMR 6174, 4 place Tharradin, F-25211 Montbéliard, France

ARTICLE INFO

Keywords:
Multilayers
Thin films
(Ti-Al-N) system
Microstructure
TEM

ABSTRACT

Radiofrequency magnetron sputtering combined with reactive gas pulsing process was used to synthesize two titanium aluminum nitride multilayer films using a periodically controlled nitrogen flow rate changing from 0.4 to 1 sccm (sample S04-1) and from 0 to 1 sccm (sample S0-1). A metallic TiAl buffer layer was deposited on the etched substrates before the deposition to enhance their adhesion. The films were characterized using mainly transmission electron microscopy and electron diffraction. The role of the crystallinity of the buffer TiAl metallic layer deposited before gas introduction on the growth orientations is emphasized. It is shown that the formation of a multilayer structure is conditioned by stopping periodically and completely the nitrogen flow rate. Particular attention is paid to the role that residual oxygen can play on the microstructure and to transient regime that occurs when the flow rate drops from 1 sccm to 0 sccm.

1. Introduction

Metalworking industry needs cutting tools with increased performance for high-speed machining and metallic nitride films are extensively used as protective coatings of cutting tools. Nowadays, the Ti-Al-N system is well known to be one of the most interesting systems to synthesize coatings for such applications [1,2]. The addition of Al into the cubic lattice of TiN films improves the oxidation and wear resistance of the coatings. The Ti-Al-N system has thus been largely studied [1–7] especially to understand the role of Al content on the nano- and micro-structure of the films and consequently on their mechanical properties. Reactive magnetron sputtering is widely used to synthesize such ternary nitrides with non-equilibrium growth conditions, which allows the formation of metastable supersaturated $Ti_{1-x}Al_xN$ films [10] generally with columnar microstructures [8,9]. More particularly, $Ti_{1-x}Al_xN$ films where Al is substituted for Ti in the face centered cubic (fcc) rock salt lattice have attracted important interest because of their improved oxidation resistance and mechanical performances [10,11]. Nevertheless, a detrimental formation of a hexagonal wurtzite-type (hcp) phase (similar to h-AlN) can occur in the coatings for large x values in $Ti_{1-x}Al_xN$. This value of x for which fcc and hcp phases can coexist in the coatings strongly depends on the deposition parameters and varies from 0.52 [12] to 0.7 [13]. The best mechanical properties are observed for coatings whose Al content is around 50% of the metallic part [14,15].

Among these hard coatings, the deposition of (Ti,Al)N-based multilayer coatings is another possibility to improve the performance by limiting the propagation of cracks [16] and thus enhancing the mechanical properties [17–20]. Several reasons argue for advantages of depositing multilayered films [21,22]. A superlattice effect is obtained for multilayers prepared with very thin layers component with the enhancement of the hardness explained by the Hall and Petch effect [23–26]. Generally, the stacking structure of these coatings is complex and must be studied precisely to understand its influence on their functionality. Transmission Electron Microscopy (TEM) is a technique of choice for such a purpose, allowing a characterization of the structure of these coatings from the atomic to micrometric scale. For example, it is largely used for cross-sectional observations of the samples to study the evolution of the microstructure (preferential orientation, columnar growth, …) during the deposition process [23,27,28]. At the atomic scale, it was used to evidence intermixing layers in (Ti,Al)N-based multilayer films [29] and their influence on the mechanical properties [30].

The present study focuses on the characterization of $(Ti,Al)N_x$/

* Corresponding author.
E-mail address: marie-jose.pac@uha.fr (M.-J. Pac).
[1] Died 2019 May 14.

https://doi.org/10.1016/j.surfcoat.2019.06.071
Received 26 March 2019; Received in revised form 3 June 2019; Accepted 24 June 2019
Available online 25 June 2019

(Ti,Al)N_y multilayers with different nitrogen proportion layers deposited by magnetron sputtering using a reactive gas pulsing process (RGPP) [31]. This technique enables the fabrication of multilayer coatings with tailored nitrogen stoichiometry from a TiAl target with a controlled and pulsing reactive N_2 flow rate. The structure of the as-deposited multilayers was studied by TEM to understand the effect of changing the nitrogen flow rate from a layer to another. By combining direct imaging, electron diffraction and Energy Dispersive X-Ray Spectroscopy (EDXS), it was possible to obtain detailed information about phase composition and orientation, grain size and shape. Wavelength dispersion spectroscopy was also used to provide complementary information about the stoichiometry of the deposited layers. On the basis of these characterizations, it clearly appears that complex phenomena occurred during the deposition process showing that some deposition parameters play a crucial role on the microstructure of the coatings.

2. Experimental conditions

Thin films, monolayers and multilayers, were deposited onto (100) silicon substrates by radiofrequency (RF) magnetron sputtering from a TiAl sintered metallic target (purity 99.99%, ratio Ti/Al = 2 and 50 mm diameter). The target was sputtered by a RF generator (13.56 MHz) with a constant power density of 4 $W{\cdot}cm^{-2}$. The distance between the target and the substrate was fixed at 60 mm. Before the sputtering process a background pressure of 10^{-5} Pa was reached in the vacuum chamber. All depositions were carried out with a constant pumping speed of 10 $L{\cdot}s^{-1}$ and an argon flow rate of 2 sccm, which produced an argon partial pressure of 0.52 Pa. Before the deposition, the native oxide layer (SiO_x) of the substrate was etched in argon plasma (1 Pa, 250 V) during 1200 s. A $Ti_{0.67}Al_{0.33}$ buffer layer was systematically deposited on the etched substrates before the film deposition to enhance its adhesion.

In this paper two types of films were studied. First, three single-layered films, S0, S04 and S1 were obtained with a total thickness close to 2000 nm and using a constant nitrogen flow rate ($Q(N_2)$) of 0, 0.4 and 1 sccm, respectively (Table 1).

Secondly, two multilayers S04-1 and S0-1 were obtained using a variable nitrogen flow rate ($Q(N_2)$ changing between 0.4 and 1 or 0 and 1 sccm, respectively (Table 1). Nitrogen flow rate was periodically controlled versus time according to a rectangular pulse by the reactive gas pulsing process (RGPP) [32,33]. The pulsing period T ($T = t_{on} + t_{off}$) of the $Q(N_2)$ was changed from 234 to 360 s to produce two different periodic alloy/nitride or nitride/nitride multilayers (Table 1). The maximum of $Q(N_2)$ was fixed at 1.0 sccm and was applied to operate in the nitride sputtering mode ((Ti,Al)N) during the t_{on} nitrogen injection time. Also, the minimum of $Q(N_2)$ was fixed at 0 or 0.4 sccm during the t_{off} time, for S0-1 and S04-1 samples, respectively. The nitrogen flow rate $Q(N_2) = 0$ sccm was fixed to operate in the alloy sputtering mode (TiAl). Otherwise, the nitrogen flow rate $Q(N_2) = 0.4$ sccm is the smallest nitrogen flow rate that can be introduced with the hope to grow a sub-stoichiometric nitride ($(Ti,Al)N_x$ with $x < 1$). From the deposition rate of single-layered films, the t_{on} and t_{off} of multilayers films were chosen to obtain an expected period Λ close to 30 nm, with $\Lambda = \lambda_{Alloy} + \lambda_{nitr1}$ or $\Lambda = \lambda_{nitr04} + \lambda_{nitr1}$, where λ_{Alloy}, λ_{nitr04} and λ_{nitr1} are the same expected thicknesses ($\lambda \approx 15$ nm) for the TiAl alloy, sub-stoichiometric nitride and stoichiometric nitride, respectively.

In order to investigate the microstructure of the coatings, many characterization techniques were carried out.

TEM was mainly used in the cross-section geometry to get deeper insights into the microstructure. Cross-sections were prepared by Focus Ion Beam (FIB) milling using a FEI Helios Nanolab G3 CX dual beam apparatus. The top surface of the samples was first protected by a Pt/C coating to prevent ion implantation at the surface of the samples during the process. Thin lamellas were extracted using 30 keV Ga + ions and a beam current of 10 nA. In order to prevent bending of the lamellas and subsequent artifacts during the thinning process, electron transparent windows suitable for TEM analysis were obtained by lowering the beam energy and intensity to 1 keV and 10 pA respectively.

Cross-sections were then analyzed in a JEOL 220FS TEM/STEM by Energy-Filtered Selected Area Electron Diffraction (EF-SAED) and Scanning Transmission Electron Microscopy (STEM). Energy Dispersive X-ray Spectroscopy (EDXS) analysis was performed with a 60 mm^2 Bruker X-Flash SDD by using an analytical Be-holder to minimize spurious signals coming from the objective pole piece area.

Annular Dark Field STEM (ADF-STEM) and High Angle Annular Dark Field (HAADF-STEM) micrographs were simultaneously acquired (probe size of 0.7 nm). The probe convergence semi-angle was 8mrad, inner-collection semi-angles for ADF and HAADF were 8 mrad and 40 mrad respectively. Informations about the crystallinity of the samples were so gathered from the diffraction contrast provided by ADF-STEM images together with their local chemical composition given by the mass-thickness contrast obtained from HAADF-STEM images. EDXS chemical profiles were acquired with a probe size of about 1 nm to investigate the distribution of the different chemical species in the thin films.

Additional information on the stoichiometry of the coatings was finally obtained by using Wavelength Dispersive Spectroscopy (WDS) in a Scanning Electron Microscope (SEM) under 10 kV and 10 nA.

3. Results and discussion

Cross-sectional TEM observations of the two multilayered samples were achieved and Fig. 1 gives typical HAADF-STEM images for the whole thickness of the coatings. For both samples, the silicon substrate can be clearly identified at the bottom as well as the TiAl buffer layer before the multilayer growth. Apart from the different buffer layers thicknesses (40 nm for S0-1 vs 59 nm for S04-1), one can immediately notice that a strong difference occurred during the growth of the two coatings. Indeed, whereas a stacking of 81 bilayers is evidenced for the whole thickness of the coating for sample S0-1 (Fig. 1-b), it progressively disappears for the sample S04-1 at a distance close to 450 nm from the buffer layer (Fig. 1-a). Considering that the sample thickness is roughly constant over the observed area, the contrasts variations observed in STEM-HAADF images are thus governed by the changes in the electronic density, which are induced by variations of stoichiometry in the sample. Therefore, the disappearance of contrasts typical of a multilayered structure for the sample S04-1 tends to prove that the

Table 1
Characteristics of the single- and multi-layered films. For single-layered films, thicknesses were measured by the step method using a mechanical profilometer "Dektak 3030" (Veeco). For multilayered films, the period Λ, the thickness of the buffer layer and the total film thickness were deduced from cross-sectional TEM observations.

	Sample	Thickness (nm) (± 20 nm)	TiAl buffer (nm) (± 2 nm)	$Q(N_2)$ (sccm)	$Pp(N_2)$ (Pa)	t_{on} (s)	t_{off} (s)	Λ (nm)
Monolayers	S0	2000	–	0	0	–	–	
	S04	2000	45	0.4	0.1	–	–	
	S1	2000	45	1	0.15	–	–	
Multilayers	S04-1	1550	59	0.4/1	0.1/0.15	183	177	17 + 17
	S0-1	2240	40	0/1	0/0.15	188	46	14 + 14

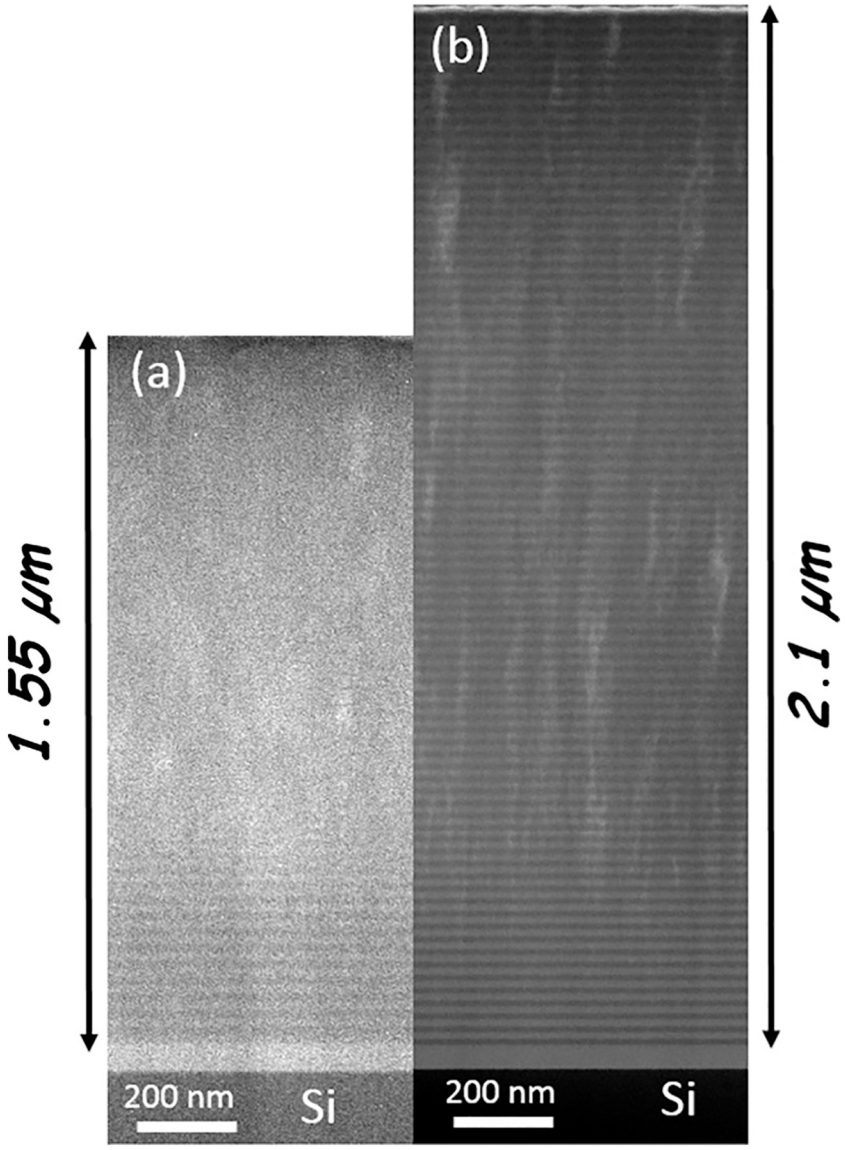

Fig. 1. Cross-sectional observations (STEM-HAADF images) of sample S04-1 (a) and S0-1 (b).

deposition conditions progressively evolved so that the growth of a homogeneous film finally occurred during the last part of the deposition process. On the contrary, for the sample S0-1, when the periodic nitrogen introduction in the deposition system was completely stopped, STEM-HAADF observations indicate that deposition conditions remain favorable for a multilayered growth all along the deposition process. Fig. 1 also shows that, in both cases, bright contrasts, elongated in the direction perpendicular to the surface, can be observed, particularly far from the substrate. Even if some of them can probably be remaining artifacts due to the fibbing process, these contrasts can mainly be attributed to a columnar growth in the coatings as it is confirmed in Fig. 2 in which STEM-ADF micrographs are displayed. On this last figure, one can observe that columnar growths occurred from the beginning of the deposition process for the S04-1 sample (Fig. 2a), whereas it only begins at 300–400 nm above the buffer layer for the S0-1 one (Fig. 2e). This columnar growth is typical of (Ti,Al)N coatings and is independent from the multilayer growth since this last is maintained up to 400 nm and up to the surface for S04-1 and S0-1 respectively. EF-SAED patterns obtained on these two samples are also given in Fig. 2. Close to the substrate, EF-SAEDP from both samples is somehow similar (Fig. 2b and f). Intense sharp spots are easily attributed to the silicon substrates while the poorly crystallized TiAl buffer layers generate the formation of quite broad diffraction rings. Elongated bows corresponding to TiAlN (200) planes of the face centered cubic (fcc) phase are also observable indicating that (Ti,Al)N layers grow with a (200) texture from the early stage of the deposition process in both cases. In fact, the only difference between the different EF-SAEDP obtained close to the substrate consists in slight reinforcements on the TiAl diffraction ring for the sample S0-1 (Fig. 2h), indicating some preferential orientation, which corresponds to TiAl (111) planes along the growth direction for this sample.

For the sample S04-1, quite simple EF-SAEDP are observed further from the silicon substrate (in the middle of the coating (Fig. 2c) and close to the surface (Fig. 2d)). Only diffraction spots ascribable to a TiAlN fcc structure with a (200) texture are observed, the diffraction spots becoming sharper closer to the top of the film. In other words, for the S04-1 sample, electron diffraction patterns characteristic of the fcc structure of a (Ti,Al)N solid solution with a (200) texture are obtained all along the deposited layer with the exception of the poorly crystallized TiAl buffer layer. Such an observation also indicates that the crystallographic structure and its preferential orientation remain very similar all along the deposition process, even for the first 400 nm for which a multilayered structure is obtained. In single-layered films, Pelleg et al. [7] were the first to propose a thermodynamic model to describe the TiN texture change depending on thickness, so-called

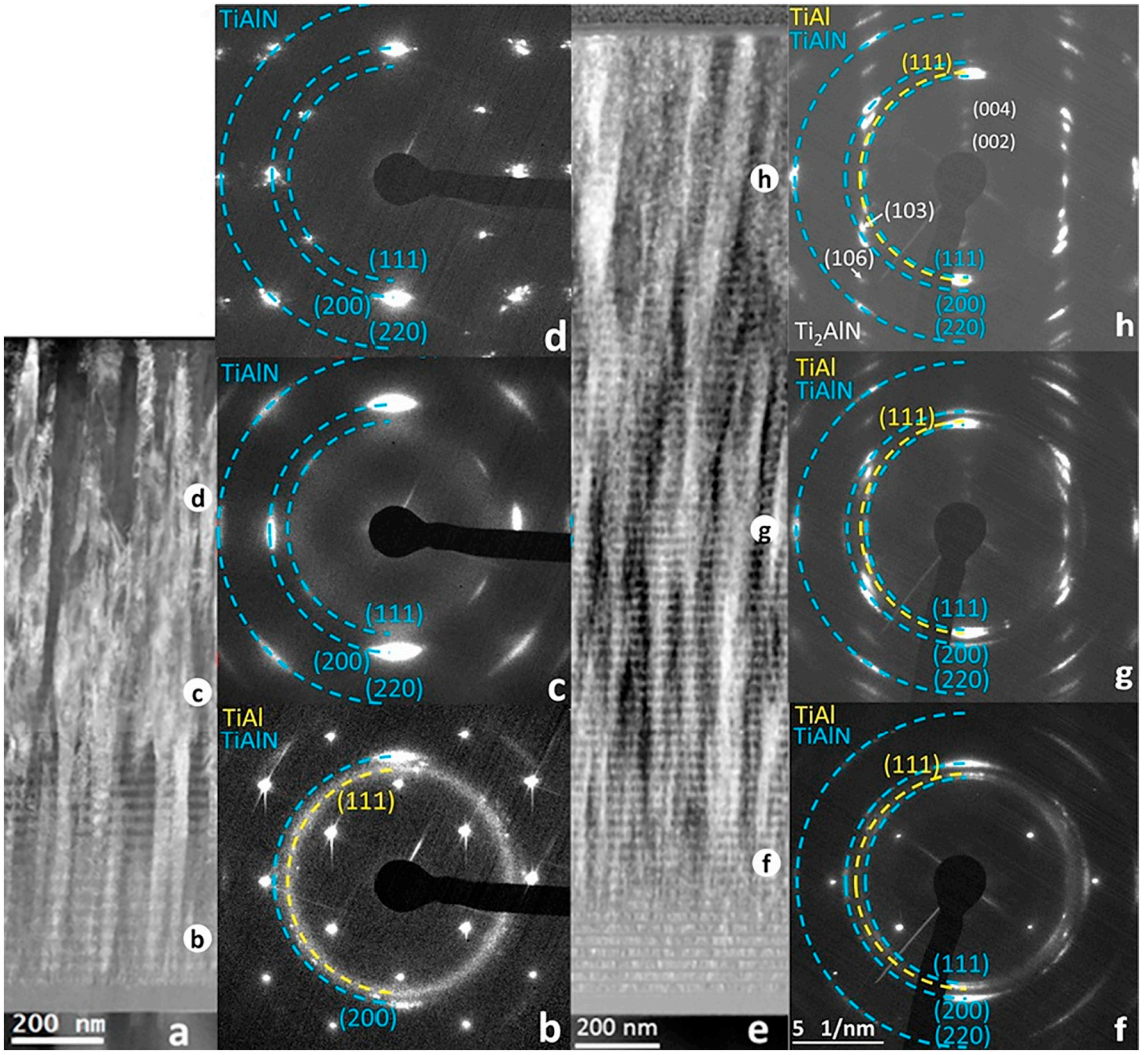

Fig. 2. STEM-ADF cross-sectional micrographs and their corresponding EF-SAEDP of sample S04-1 (a to d) and S0-1 (e to h); b) and e) close to the buffer, c) and g) middle of the film, d) and h) close to the surface. Location of the position for center of the aperture diaphragm (400 nm in diameter) used for EF-SAEDP are indicated on STEM-ADF micrographs by using corresponding letters.

"orientational crossover". According to their model, the film tends to minimize its free energy at low thickness and the growth of (001) planes with the lowest surface energy is predominant. At higher thickness, the stress contribution within the film plays a major role and the strain energy determines the preferred (111) orientation of the grains. Nevertheless, this model does not match with the present case for which the (200) texture had persisted even for a large thickness (1.55 μm). Finally, for the S04-1 sample, the grain size growth in the V-shaped column easily explains the sharpening of the diffraction spots closer to the surface. The V-shaped columns are typical of competitive growth [34] and already observed in several ternary systems like AlN/TiN [35] and TiN/ZrN [36].

A more complex evolution of the EF-SAEDP is obtained for the S0-1 sample (Fig. 2f to h). For this sample, EF-SAEDP can be fully indexed by using three different crystallographic structures: the fcc structure of a (Ti,Al)N solid solution, the tetragonal structure for TiAl and, more surprisingly, the hexagonal structure of the MAX phase Ti_2AlN for which the (0001) planes are parallel to TiAl(111) ones according to Blackburn's relationship [37]. As already mentioned, at the early stage of growth, the TiAl buffer layer as well as the first layers of TiAl are poorly crystallized and this explains the observation of a diffuse diffraction ring. This is confirmed by High Resolution Transmission Electron (HRTEM) observations of the buffer layers and of very first TiAl layers of the multilayer (not shown here). This diffuse ring completely disappears when the columnar growth begins and intense diffraction spots ascribable to electron diffraction on TiAl (111) planes of a quadratic phase (JCPDS number 03–065-5414) are observed on EF-SAEDP, TiAl (111) planes being perpendicular to the growth direction. A progressive crystallization of the TiAl layers thus occurred during the growth process. It is interesting to note that the best crystallized TiAl layers are located not only at the bottom of the columnar growth of the grains but also they correspond to the change of the preferential crystallographic orientation for the fcc (Ti,Al)N layers. For the fcc (Ti,Al)N phase, Fig. 2g and h show that the (200) preferential orientation progressively disappeared during the growth process while the (111) texture became prominent. These observations allow concluding that the columnar growth occurred through the multilayer system with a preferential TiAl(111)/(Ti,Al)N (111) orientation relationship between the layers.

In addition to diffraction spots that can be attributed to the presence of fcc (Ti,Al)N and tetragonal TiAl phases, some weak extra diffraction spots can be observed on Fig. 2g and h, which can be indexed by using the hexagonal structure of the MAX phase Ti_2AlN. The formation of the latter was already observed in TiAl/TiN multilayers deposited at room temperature by Dolique et al [40] but only after an annealing at 600 °C. In this last work, thanks to interdiffusion phenomena that take place

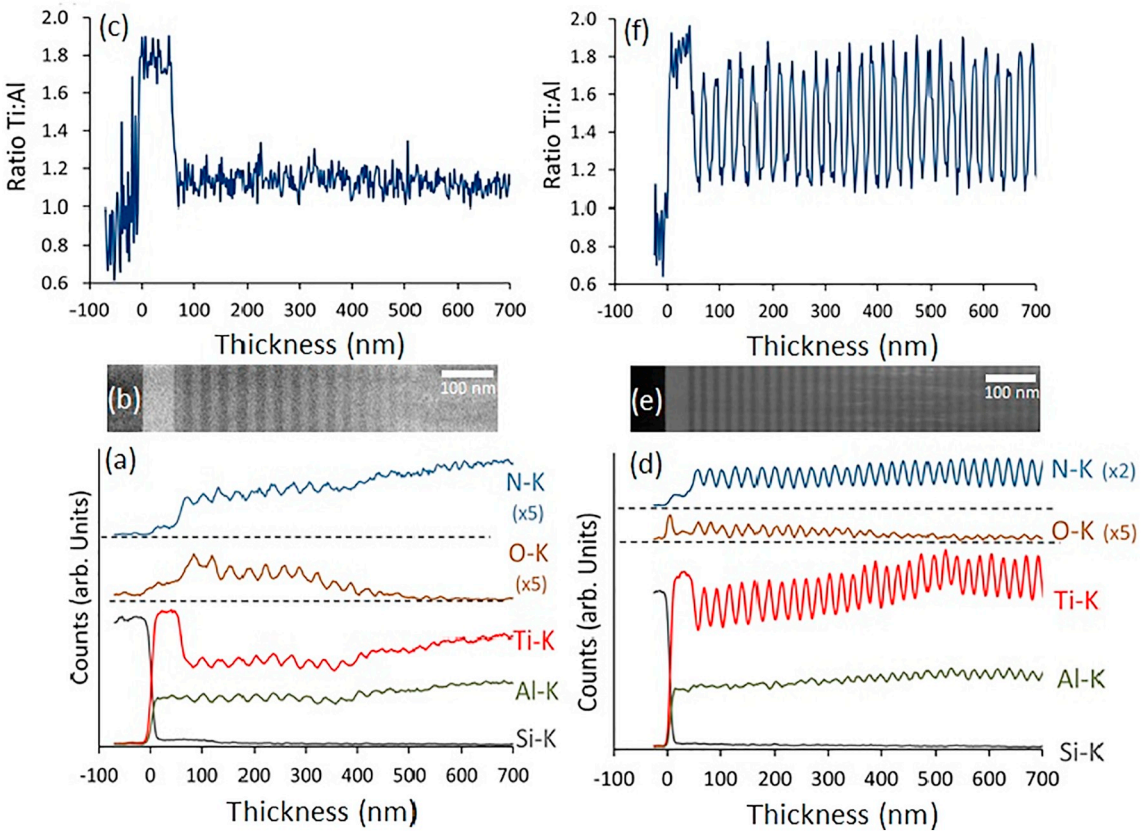

Fig. 3. EDXS analysis ((a) and (d)), Ti:Al ratio ((c) and (f)) and corresponding STEM-HAADF micrographs (b) and (e) for sample S04-1 and S0-1 respectively; for ease of reading, N and O signals were shifted upward.

during the holding at higher temperature, a full transformation of the TiAl layers into the MAX phase Ti_2AlN was likely achieved. In the present work, neither HRTEM nor dark field observations allow to identify where the formation of this phase takes place. The very low intensity of the diffraction spots from the MAX phase in the EF-SAEDP suggests that it is present in very small amount.

To better understand the evolution of the microstructure for both samples, EDXS analysis was conducted in the STEM mode (Fig. 3). For the sample S04-1 (Fig. 3a), with the exception of the buffer layer for which it is close to 1.8, the Ti:Al ratio keeps a value close to 1.1 all along the thickness of the film, whatever the nitrogen pressure in the deposition chamber. On the contrary, strong variations of the nitrogen concentration are obtained for the first 450–500 nm of the layer and more surprisingly a significant oxygen signal is observed whose integrated intensity varies in anticorrelation with the nitrogen one. Indeed, larger nitrogen concentrations and thus smaller oxygen one are observed for layers deposited with the lower nitrogen flow rate (0.4 sccm) in the deposition chamber, while it is the opposite for the layers deposited with a larger nitrogen flow rate (1 sccm). Unfortunately, this clearly indicates that some oxygen contamination was present in the nitrogen circuit at the first stage of the deposition process and that unwanted phenomenon is at the origin of the multilayer structure observed for the first 450–500 nm. More precisely, at the beginning of the deposition process, the oxygen partial pressure in the vacuum chamber increases for larger nitrogen flow rate and a larger amount of oxygen atoms are incorporated into the growing film thanks to their strong chemical affinity with Ti and Al atoms. As a consequence, the incorporation of N atoms decreases at the same time. Interestingly, the crystallographic structure (rock salt structure) as well as the preferential orientation (200) of the growing layers is kept whatever the O:N ratio while HAADF observation (Fig. 1a) indicates that oxygen-rich layers have a lower electronic density. The incorporation of oxygen into $TiN_{1-x}O_x$ layers is known to decrease the lattice parameters of the fcc structure so obtained [38] while it is the opposite for $TiAlN_{1-x}O_x$ compounds [39]. That is not in good agreement with the results obtained by Zhu et al. who claimed that the more oxygen flow rate is introduced in TiAlN structure the more the lattice parameter decreases; however, they did not mention if injecting higher oxygen flow rate led to higher proportion of oxygen in the film [40]. Furthermore, on the basis of the here presented results, it is not possible to conclude that $(Ti,Al)N_xO_y$ compounds with $x + y = 1$ are obtained. More specifically, oxygen and nitrogen concentrations can be so that $x + y < 1$. In other words, the incorporation of oxygen into the growing (Ti,Al)N layers possibly contributed to a decrease in their electronic density and would so explain HAADF observation as that shown in Fig. 1a where darker layers are oxygen-rich.

EDXS characterization thus allows a better understanding of the microstructural evolution of the layer and of the different phenomena that take place during the deposition of the S04-1 sample. A multilayered structure is only obtained up to 450 nm when variations of non-negligible amounts of oxygen exist inside the coating. In contrast, from 450 to 1550 nm, without any oxygen incorporation in the coating, simple variations of the nitrogen flow rate from 1 sccm to 0.4 sccm only allow the growth of a layer with an almost constant stoichiometry (Fig. 3a) and do not allow the development of a multilayer film. Such an observation is somehow surprising since one can expect variations of the composition of the growing film when the nitrogen partial pressure is decreased from 0.16 Pa for $QN_2 = 1$ sccm to 0.07 Pa for $QN_2 = 0.4$ sccm. Despite this change of partial pressure, the deposition conditions appear to remain very similar when the nitrogen flow rate switched between 0.4 sccm and 1 sccm, respectively. Therefore, it can be noted that for Q (N_2) = 1 sccm and Q (N_2) = 0.4 scmm the sputtering mode does not change and operates only in nitride sputtering mode. More especially, during the time T_{off}, for which Q (N_2) = 0.4 sccm, the

Table 2
Ti, Al and N atomic concentrations deduced from WDS analysis for samples S0, S04 and S1. Reproducibility for every element is typically of the order of 1%. Ti:Al, Ti:N, and Al:N ratio are also given.

Coating	% Ti	% Al	% N	Ti:Al	Ti:N	Al:N
S0	64	36	0	1.78	–	–
S04	25.50	23.20	51.30	1.10	0.50	0.45
S1	25.60	22.70	51.60	1.13	0.50	0.44

surface of the target remains poisoned by the nitrogen preventing the possibility of elaborating a nitride sub-stoichiometric ((Ti, Al) N_x with $x < 1$) [41]. The WDS results obtained on 2 µm thick single layer deposited with the three different nitrogen flow rate 0, 0.4 and 1 sccm are presented in Table 2 and confirm this hypothesis. More especially, very similar Ti:N and Al:N ratio are obtained for the S04 and S1 samples indicating that variations of the nitrogen flow rate from 0.4 sccm to 1 sccm will not allow the formation of a multilayer structure with variable nitrogen content layers.

STEM-EDXS results obtained on the S0-1 sample, for which the multilayered structure is maintained all along the growth process, are given Fig. 3d, f. When nitrogen flow rate is fixed at 1 sccm during the deposition process, a (Ti,Al)N layer with a Ti:Al ratio close to 1.1 is obtained, as for the S04-1 sample. This Ti:Al ratio reaches a value close to 1.8 for the layers obtained when no nitrogen is introduced in the deposition chamber. Again, some small quantities of oxygen are incorporated at the beginning of the deposition process and only inside the (Ti,Al)N layers confirming a possible contamination by some residual oxygen of the nitrogen supply circuit. As for the S04-1 sample, a microstructural modification (Fig. 2e) can be associated with the loss of the oxygen content in the layer since it corresponds to the beginning of a columnar growth and to a better crystallization of the TiAl layers. Furthermore, EDXS results do not indicate the presence of oxygen in TiAl layers but one cannot exclude that the combined presence of very small quantities of oxygen and nitrogen in the TiAl layers inhibits their crystallization. Unfortunately, there is no literature dedicated to the influence of oxygen and/or nitrogen incorporation into TiAl layers, as far as the authors know, to assess this proposition. The presence of some residual nitrogen into TiAl layers is difficult to prove based on EDXS results. Nevertheless, when comparing HAADF-STEM and ADF-STEM observations as shown Fig. 4, crystallized (Ti,Al)N layers appear clearly thicker than TiAl ones indicating the presence of a non-negligible amount of nitrogen even when the nitrogen flow rate has a null value. Furthermore, incorporation of nitrogen in the TiAl layers has been previously revealed thanks to electron energy loss spectroscopy measurements performed on similar TiAl/TiAlN multilayers [25]. More especially, Fig. 4 shows that the formation of the fcc-TiAlN structure still occurred for a long time after shutting off the nitrogen flow rate. This asymmetry can first be explained by transient regimes after turning on (t_{on}) or off (t_{off}) the nitrogen introduction. As shown in Fig. 4c, the total pressure (Ar + N_2) in the deposition chamber progressively reaches 0.68 Pa when the nitrogen flow rate is 1 sccm and only 0.50 Pa without nitrogen introduction. A transition time of 20 s is observed when the pressure increases while it is only 12 s when it decreases. Nevertheless, the deposition rate for the (Ti,Al)N layers, in a poisoned mode for the target, is much lower than that of TiAl layers deposited in an alloy mode. The transition time corresponds to 10 and 26% of the deposition time of (Ti,Al)N and TiAl layers respectively. In other words, residual nitrogen partial pressure remains quite high or non-negligible for at least one quarter of the TiAl Layer. Such an observation also indicates that a TiAl/TiAlN multilayer can only be obtained for deposition time of the TiAl layers long enough to reset the deposition conditions close to the initial ones.

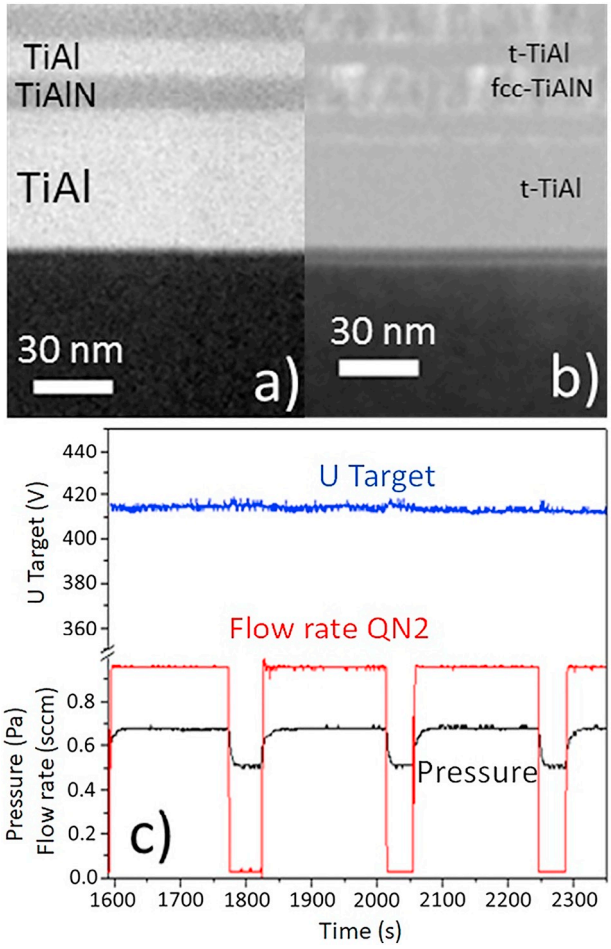

Fig. 4. STEM-HAADF (a) and STEM-ADF (b) observations for sample S0-1, c) deposition parameters: red: controlled pulsing N_2 flow rate, black: total pressure (Ar + N_2) in the deposition chamber, blue: target voltage. (For interpretation of the references to colour in this figure legend, the reader is referred to the web version of this article.)

4. Conclusion

In this work, the structure of two (Ti,Al)N coatings elaborated by magnetron sputtering using RGPP technique was characterized at micro- and nano-scales using TEM and discussed. These two coatings were deposited under periodically varied nitrogen flow rate in order to obtain a multilayer structure with varied nitrogen stoichiometry. For the first coating (S04-1), the nitrogen flow rate was switched between 0.4 sccm and 1 sccm allowing the formation of a multilayer structure but only for the first 450 nm, due to the presence of residual oxygen at the beginning of the deposition process. For this sample, the formation of a homogenous structure in the absence of oxygen proved that the difference between the nitrogen flow rates did not allow variations of the stoichiometry large enough for the formation of a multilayered structure. For the second sample, for which the nitrogen flow rate was completely cut off, a multilayer structure was obtained over the entire thickness of the coating confirming that the RGPP can be considered as a quite powerful method for the synthesis of multilayers in the (Ti,Al)N system.

In the two coatings, a columnar growth was observed at two different thicknesses; from the beginning for the S04-1 sample and above 200–300 nm for the S0-1 one, probably due the presence of oxygen preventing the crystallization of TiAl. Several crystallographic orientations were indexed in the SAEDP, which evolved with the film thickness. For S04-1, (Ti,Al)N cubic phase had a {200} orientation over

the whole thickness, while for S0-1, the growth began with a {200} orientation and switch to {111} as the TiAl tetragonal phase evolved in this last orientation also. In this sample, TiAl and (Ti,Al)N layers seemed to not have the same thickness because of transitional regimes after shutting on or off the nitrogen introduction. TiAl/TiAlN multilayered films can thus only be obtained for long enough deposition time for the TiAl layers since residual nitrogen partial pressure remains quite high during a significant part of the deposition time of TiAl layer.

Declaration of Competing Interest

None.

Acknowledgement

This work was partially funded by the French Government Program “Investissements d'Avenir” (LABEX INTERACTIFS, reference ANR-11-LABX-0017-01). The authors thank also the community PMA “Pays Montbeliard Agglomération” for financial support (Contrat 20161016061).

References

[1] S. PalDey, S.C. Deevi, Single layer and multilayer wear resistant coatings of (Ti,Al)N: a review, Mater. Sci. Eng. A 342 (2003) 58–79, https://doi.org/10.1016/S0921-5093(02)00259-9.
[2] H.W. Hugosson, H. Högberg, M. Algren, M. Rodmar, T.I. Selinder, Theory of the effects of substitutions on the phase stabilities of $Ti_{1-x}Al_xN$, J. Appl. Phys. 93 (2003) 4505, https://doi.org/10.1063/1.1557779.
[3] M. Zhou, Y. Makino, M. Nose, K. Nogi, Phase transition and properties of Ti-Al-N thin prepared by r.f.-plasma assisted magnetron sputtering, Thin Solid Films 339 (1999) 203–208, https://doi.org/10.1016/S0040-6090(98)01364-9.
[4] F. Vaz, L. Rebouta, M. Andritschky, M.F. da Silva, J.C. Soares, Thermal oxidation of Ti1 − xAlxN coatings in air, J. Eur. Ceram. Soc. 17 (1997) 1971–1977, https://doi.org/10.1016/S0955-2219(97)00050-2.
[5] D. Rafaja, A. Poklad, V. Klemm, G. Schreiber, D. Heger, M. Šíma, M. Dopita, Some consequences of the partial crystallographic coherence between nanocrystalline domains in Ti-Al-N and Ti-Al-Si-N coatings, Thin Solid Films 514 (2006) 240–249, https://doi.org/10.1016/j.tsf.2006.02.092.
[6] A. Höling, L. Hultman, M. Odén, J. Sjölén, L. Karlsson, Mechanical properties and machining performance of Ti1-xAlxN-coated cutting tools, Surf. Coatings Technol. 191 (2005) 384–392, https://doi.org/10.1016/j.surfcoat.2004.04.056.
[7] A. Kimura, M. Kawate, H. Hasegawa, T. Suzuki, Anisotropic lattice expansion and shrinkage of hexagonal TiAlN and CrAlN films, Surf. Coatings Technol. 169–170 (2003) 367–370, https://doi.org/10.1016/S0257-8972(03)00040-9.
[8] P.H. Mayrhofer, D. Music, J.M. Schneider, Influence of the Al distribution on the structure, elastic properties, and phase stability of supersaturated Ti1-xAlxN, J. Appl. Phys. 100 (2006) 094906, , https://doi.org/10.1063/1.2360778.
[9] M.-H. Tuilier, M.-J. Pac, G. Covarel, C. Rousselot, L. Khouchaf, Structural investigation of thin films of $Ti_{1-x}Al_xN$ ternary nitrides using Ti K-edge X-ray absorption fine structure, Surf. Coat. Technol. 201 (2007) 4536–4541, https://doi.org/10.1016/j.surfcoat.2006.09.095.
[10] A. Kimura, H. Hasegawa, K. Yamada, T. Suzuki, Effects of Al content on hardness, lattice parameter and microstructure of $Ti_{1-x}Al_xN$ films, Surf. Coatings Technol. 121 (1999) 438–441.
[11] K. Kutschej, P.H. Mayrhofer, M. Kathrein, P. Polcik, R. Tessadri, C. Mitterer, Structure, mechanical and tribological properties of sputtered $Ti_{1-x}Al_xN$ oatings with $0.5 \leq x \leq 0.75$, Surf. Coatings Technol. 200 (2005) 2358–2365, https://doi.org/10.1016/j.surfcoat.2004.12.008.
[12] U. Wahlström, L. Hultman, J.E. Sundgren, F. Adibi, I. Petrov, J.E. Greene, Crystal growth and microstructure of polycrystalline $Ti_{1-x}Al_xN$ alloy films deposited by ultra-high-vacuum dual-target magnetron sputtering, Thin Solid Films 235 (1993) 62–70, https://doi.org/10.1016/0040-6090(93)90244-J.
[13] D. Rafaja, M. Šíma, V. Klemm, G. Schreiber, D. Heger, L. Havela, R. Kužel, X-ray diffraction on nanocrystalline $Ti_{1-x}Al_xN$ thin films, J. Alloys Compd. 378 (2004) 107–111, https://doi.org/10.1016/j.jallcom.2003.10.087.
[14] M.-J. Pac, S. Giljean, C. Rousselot, F. Richard, P. Delobelle, Microstructural and elasto-plastic material parameters identi fi cation by inverse fi nite elements method of $Ti(1-x)Al_xN$ ($0 < x < 1$) sputtered thin fi lms from Berkovich nano-indentation experiments, Thin Solid Films 569 (2014) 81–92, https://doi.org/10.1016/j.tsf.2014.07.037.
[15] C. Wüstefeld, D. Rafaja, V. Klemm, C. Michotte, M. Kathrein, Effect of the aluminium content and the bias voltage on the microstructure formation in $Ti_{1x}Al_xN$ protective coatings grown by cathodic arc evaporation, Surf. Coat. Technol. 205 (2010) 1345–1349, https://doi.org/10.1016/j.surfcoat.2010.07.057.
[16] H. Holleck, V. Schier, Multilayer PVD coatings for wear protection, Surf. Coatings Technol. 76–77 (1995) 328–336, https://doi.org/10.1016/0257-8972(95)02555-3.
[17] K.N. Andersen, E.J. Bienk, K.O. Schweitz, H. Reitz, J. Chevallier, P. Kringhøj, J. Bøttiger, Deposition, microstructure and mechanical and tribological properties of magnetron sputtered TiN/TiAlN multilayers, Surf. Coatings Technol. 123 (2000) 219–226, https://doi.org/10.1016/S0257-8972(99)00473-9.
[18] J.M. Castanho, M.T. Vieira, Effect of ductile layers in mechanical behaviour of TiAlN thin coatings, J. Mater. Process. Technol. 143–144 (2003) 352–357, https://doi.org/10.1016/S0924-0136(03)00454-0.
[19] W. Tillmann, E. Vogli, S. Momeni, Mechanical and tribological properties of Ti/TiAlN duplex coatings on high and low alloy tool steels, Vacuum 84 (2009) 387–392, https://doi.org/10.1016/j.vacuum.2009.08.001.
[20] E. Vogli, W. Tillmann, U. Selvadurai-Lassl, G. Fischer, J. Herper, Influence of Ti/TiAlN-multilayer designs on their residual stresses and mechanical properties, Appl. Surf. Sci. 257 (2011) 8550–8557, https://doi.org/10.1016/j.apsusc.2011.05.013.
[21] O. Knotek, F. Löffler, G. Krämer, Process and advantage of multicomponent and multilayer PVD coatings, Surf. Coatings Technol. 59 (1993) 14–20, https://doi.org/10.1016/0257-8972(93)90048-S.
[22] W.D. Sproul, Multilayer, multicomponent, and multiphase physical vapor deposition coatings for enhanced performance, J. Vac. Sci. Technol. A Vacuum, Surfaces, Film. 12 (1994) 1595–1601, https://doi.org/10.1116/1.579361.
[23] M.-J. Pac, Y. Pinot, S. Giljean, C. Rousselot, P. Delobelle, C. Ulhaq-Bouillet, M.-H. Tuilier, Investigation of $Ti_{0.54}Al_{0.46}/Ti_{0.54}Al_{0.46}N$ multilayer films deposited by reactive gas pulsing process by nano-indentation and electron energy-loss spectroscopy, Thin Solid Films 634 (2017) 96–106, https://doi.org/10.1016/j.tsf.2017.05.015.
[24] X. Chu, S.A. Barnett, M.S. Wong, W.D. Sproul, Reactive unbalanced magnetron sputter deposition of polycrystalline TiN/NbN superlattice coatings, Surf. Coatings Technol. 57 (1993) 13–18, https://doi.org/10.1016/0257-8972(93)90331-H.
[25] E.O. Hall, The deformation and ageing of mild steel, Proc. Phys. Soc. London Sect. B. 64 (1951) 747–753, https://doi.org/10.1088/0370-1301/64/9/303.
[26] M. Kato, T. Moris, L.H. Schwartz, Hardening by spinodal modulated structure, Acta Mater. 28 (1980) 285–290.
[27] Y. Pinot, M.-J. Pac, P. Henry, C. Rousselot, Y.I. Odarchenko, D.A. Ivanov, C. Ulhaq-bouillet, O. Ersen, M.-H. Tuilier, Friction behaviour of TiAlN fi lms around cubic/hexagonal transition: a 2D grazing incidence X-ray diffraction and electron energy loss spectroscopy study, Thin Solid Films 577 (2015) 74–81, https://doi.org/10.1016/j.tsf.2015.01.044.
[28] Y. Pinot, M.-H. Tuilier, M.-J. Pac, C. Rousselot, D. Thiaudière, Influence of film thickness on the structural transition cubic/hexagonal within $Ti_{0.38}Al_{0.62}N$ films, Thin Solid Films 649 (2018) 160–166, https://doi.org/10.1016/j.tsf.2018.01.024.
[29] H. Meidia, A.G. Cullis, C. Schonjahn, W.D. Munz, J.M. Rodenburg, Investigation of intermixing in TiAlN/VN nanoscale multilayer coatings by energy-filtered TEM, Surf. Coat. Techn ol. 152 (2002) 209–213.
[30] J.S. Yoon, H.Y. Lee, J.G. Han, S.H. Yang, J. Musil, The effect of Al composition on the microstructure and mechanical properties of WC.TiAlN superhard composite coating, Surf. Coat. Technol. 142 (2001) 596–602.
[31] N. Martin, J. Lintymer, F. Sthal, O. Banakh, H. le Dréo, P.A. Steinman, M. Fenker, H. Kappl, C. Rousselot, C. Petitjean, M. Grafouté, P.A. Cavaleiro, N. Parreira, T. Polcar, F. Vaz Carvalho, L. Rebouta, Procédé de pulvérisation réactive à signal de commande cyclique et dispositif correspondant, FR2905124, (2008).
[32] N. Martin, Procédé de pulvérisation réactive à signal de commande cyclique et dispositif correspondant, (2006), p. 0607542.
[33] A.J. Aronson, D. Chen, W.H. Class, Preparation of titanium nitride by a pulsed D.C. magnetron reactive deposition technique using the moving mode of deposition, Thin Solid Films 72 (1980) 535–540.
[34] M. Beckers, N. Schell, R.M.S. Martins, A. Mücklich, W. Möller, In situ x-ray diffraction studies concerning the influence of Al concentration on the texture development during sputter deposition of Ti–Al – N thin films, J. Vac. Sci. Technol. A Vacuum, Surfaces, Film. 23 (2005) 1384, https://doi.org/10.1116/1.2011400.
[35] Y.Y. Wang, Synthesis and characterization of highly textured polycrystalline AlN/TiN superlattice coatings, J. Vac. Sci. Technol. A Vacuum, Surfaces, Film. 16 (1998) 3341, https://doi.org/10.1116/1.581542.
[36] S. Ulrich, C. Ziebert, M. Stüber, E. Nold, H. Holleck, M. Göken, E. Schweitzer, P. Schlooßmacher, Correlation between constitution, properties and machining performance of TiN/ZrN multilayers, Surf. Coatings Technol. 188–189 (2004) 331–337, https://doi.org/10.1016/j.surfcoat.2004.08.056.
[37] M.J. Blackburn, The Science, Technology and Applications of Titanium, Pergamon P, 1970.
[38] M. Radecka, E. Pamula, A. Trenczek-zajac, K. Zakrzewska, A. Brudnik, E. Kusior, Chemical compositio, crystallographic structure and impedance spectroscopy of titanium oxynitride TiNxOy thin fi lms, Solid State Ionics 192 (2011) 693–698, https://doi.org/10.1016/j.ssi.2010.07.021.
[39] M. Baben, L. Raumann, J.M. Schneider, Phase stability and elastic properties of titanium aluminum oxynitride studied by ab initio calculations, J. Phys. D. Appl. Phys. 46 (2013), https://doi.org/10.1088/0022-3727/46/8/084002.
[40] D. Zhu, F. Mao, S. Zhao, Solar energy materials & solar cells the influence of oxygen in TiAlOxNy on the optical properties of colored solar-absorbing coatings, Sol. Energy Mater. Sol. Cells 98 (2012) 179–184, https://doi.org/10.1016/j.solmat.2011.11.001.
[41] A. Farhaoui, A. Bousquet, R. Smaali, A. Moreau, E. Centeno, J. Cellier, C. Bernard, R. Rapegno, F. Réveret, E. Tomasella, Reactive gas pulsing sputtering process, a promising technique to elaborate silicon oxynitride multilayer nanometric antireflective coatings, J. Phys. D. Appl. Phys. 50 (2017) 1–9, https://doi.org/10.1088/1361-6463/50/1/015306.